REPORT DOCUMENTATION PAGE

Form Approved
OMB No. 0704-0188

1. AGENCY USE ONLY (Leave blank)	2. REPORT DATE	3. REPORT TYPE AND DATES COVERED
	June 26, 1991	Reprint

4. TITLE AND SUBTITLE
A Wavefront Sensor for Extended, Incoherent Targets

5. FUNDING NUMBERS
PE 61102F
PR 2311
TA G3
WU 22

6. AUTHOR(S)
O. von der Luhe

7. PERFORMING ORGANIZATION NAME(S) AND ADDRESS(ES)
Phillips Lab/PHS
Hanscom AFB
Massachusetts 01731-5000

8. PERFORMING ORGANIZATION REPORT NUMBER
PL-TR-91-2151

9. SPONSORING/MONITORING AGENCY NAME(S) AND ADDRESS(ES)

10. SPONSORING/MONITORING AGENCY REPORT NUMBER

11. SUPPLEMENTARY NOTES
Reprinted from LEST Foundation Proceedings of the Workshop on Adaptive Optics in Solar Observations, Technical Report No. 28 December 1987

12a. DISTRIBUTION/AVAILABILITY STATEMENT
Approved for public release; Distribution unlimited

12b. DISTRIBUTION CODE

13. ABSTRACT (Maximum 200 words)

I propose a novel method for sensing wavefront errors in an aberrated solar telescope. The wavefront sensor consists of a transparent mask located at an image plane. A difference image of the scene under observation is encoded in density on the mask. Wavefront error slopes can be detected in a pupil image following the mask in the form of intensity variations.

The principle of the method is described and results of one-dimensional simulation calculations are presented. The technical implementation of the method is discussed as well as the effect of photon noise on the slope measurement. It is demonstrated that the proposed method is very sensitive and requires only a few percent of the incident light for a photon-noise limited null state measurement.

14. SUBJECT TERMS	15. NUMBER OF PAGES
Solar instrumentation, Active optics, Wavefront sensor	13
	16. PRICE CODE

17. SECURITY CLASSIFICATION OF REPORT	18. SECURITY CLASSIFICATION OF THIS PAGE	19. SECURITY CLASSIFICATION OF ABSTRACT	20. LIMITATION OF ABSTRACT
Unclassified	Unclassified	Unclassified	SAR

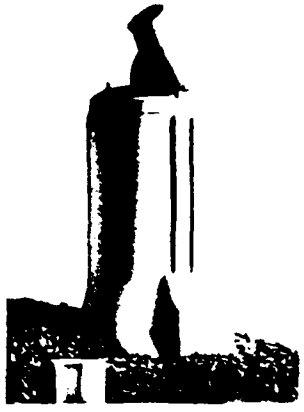

LEST Foundation

An international organization for a Large Earth-based Solar Telescope

TECHNICAL REPORT NO. 28

PROCEEDINGS OF THE WORKSHOP ON ADAPTIVE OPTICS IN SOLAR OBSERVATIONS

September 8-9, 1987, Freiburg

Editors:
F.Merkle, O.Engvold, R.Falomo

1987

The Technical Report Series is published at
Institute of Theoretical Astrophysics,
University of Oslo
Editors: O. ENGVOLD and Ø. HAUGE
Editorial assistant: L.J. JENSEN

ISSN 0800-7780

A Wavefront Sensor for Extended, Incoherent Targets

O. von der Lühe

Air Force Geophysics Laboratoty
Solar Research Branch
Sunspot, NM 88349
USA

ABSTRACT

I propose a novel method for sensing wavefront errors in an aberrated solar telescope. The wavefront sensor consists of a transparent mask located at an image plane. A difference image of the scene under observation is encoded in density on the mask. Wavefront error slopes can be detected in a pupil image following the mask in the form of intensity variations.

The principle of the method is described and results of one-dimensional simulation calculations are presented. The technical implementation of the method is discussed as well as the effect of photon noise on the slope measurement. It is demonstrated that the proposed method is very sensitive and requires only a few percent of the incident light for a photon-noise limited null state measurement.

1. Introduction

Wavefront sensors generally operate on confined targets, sometimes assumed to be point sources, such as bright stars or target glints. Consequently, a solar adaptive optic often works with small, high contrast structures such as small sunspots or pores. The construction of a wavefront sensor for more general targets, like, e. g., solar granulation is difficult and expensive if conventional concepts are used. For example, a Hartmann-type wavefront sensor that operates on granulation presumably requires one correlation tracker for each subaperture channel and might be costly.

This paper describes a wavefront sensor that is based on a novel principle of wavefront detection which is particularly well suited for extended, incoherent sources (von der Lühe, 1987). The wavefront sensor consists of a transparent "mask" in an image plane of the telescope, followed by optics that reimage the instrument's entrance pupil (fig. 1). Given a suitable transmittance distribution of the mask that is based on partial knowledge of the fine structure present in the target region, wavefront deformations can be measured in the pupil image in form of fluctuations in intensity. The proposed device results in a sensitive technique to measure the atmospheric and instrumental aberrations of a solar telescope.

The principle of the method is described in the next section. Numerical simulations are presented in section 3. A possible way to realize a wavefront sensor for a solar adaptive optic based on the technique is discussed in section 4 and a signal-to-noise ratio analysis for photon noise is done in section 5.

2. Principle of the technique

The basic optical layout of the method is shown in fig. 1. The target structure (surface of the sun) is located in the plane labeled O. An optical system that has an entrance pupil in P forms an image of O in the focal plane O'. Additional optics reimage the entrance pupil plane P to P'. Suppose that the intensity distribution in O is given by $I(\mathbf{x})$, where $\mathbf{x}$ is a two-dimensional coordinate. For the sake of simplicity, coordinates $\mathbf{x}$ will be used to designate object points as well as image points. We insert a transparent screen (the "mask") into the focal plane O'. The mask's transmittance $m(\mathbf{x})$ shall be given by:

$$m(\mathbf{x}) = B + C \left(I(\mathbf{x} - \Delta) - I(\mathbf{x} + \Delta) \right) \qquad (1)$$

The constants B and C are chosen such as to limit the mask's transparency between 0 and 1. The fixed shift Δ is chosen not larger than the correlation scale of the target

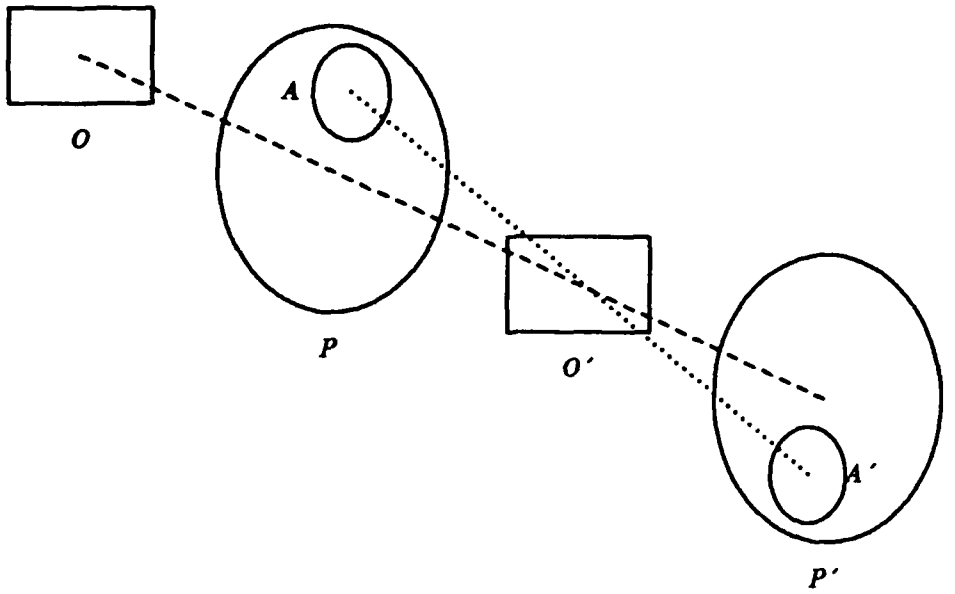

Fig. 1

Optical layout of the proposed method.

structure, i. e., the correlation scale of granulation (some 1.5 arc seconds). Fig. 2 presents a 10x10 arc second section of the photosphere (upper section) and a difference picture according to eqn. (1) (lower left section) where the shift Δ corresponds to 0.5 arcseconds in the horizontal direction.

In order to understand how the technique works, let us assume that the wavefront error consists of a purely linear term, i. e., there is only a displacement of the focal plane image. We place a detector into P' that measures the total intensity in the pupil image following the mask. If there is no displacement, we will measure a certain integral intensity in P'. If the image moves in the Δ - direction, bright portions in the field will coincide with sections in the mask that have higher transmission, so the overall measured intensity will increase. The opposite holds if the focal plane image moves in the $-\Delta$ - direction. We can therefore measure overall image shift parallel to Δ by measuring the integral intensity in P'. A second device having a mask shift Δ' perpendicular to Δ measures image displacements in the orthogonal direction.

This principle is easily extended to the measurement of local wavefront tilt. Consider a section A in the entrance pupil of the telescope and its image A' in P' (fig. 1). The section A will form an image of the target structure on the mask, displaced according to the local wave front tilt averaged over the area of A. The displacement can be measured as a change in intensity averaged over the area A'. The distribution of the

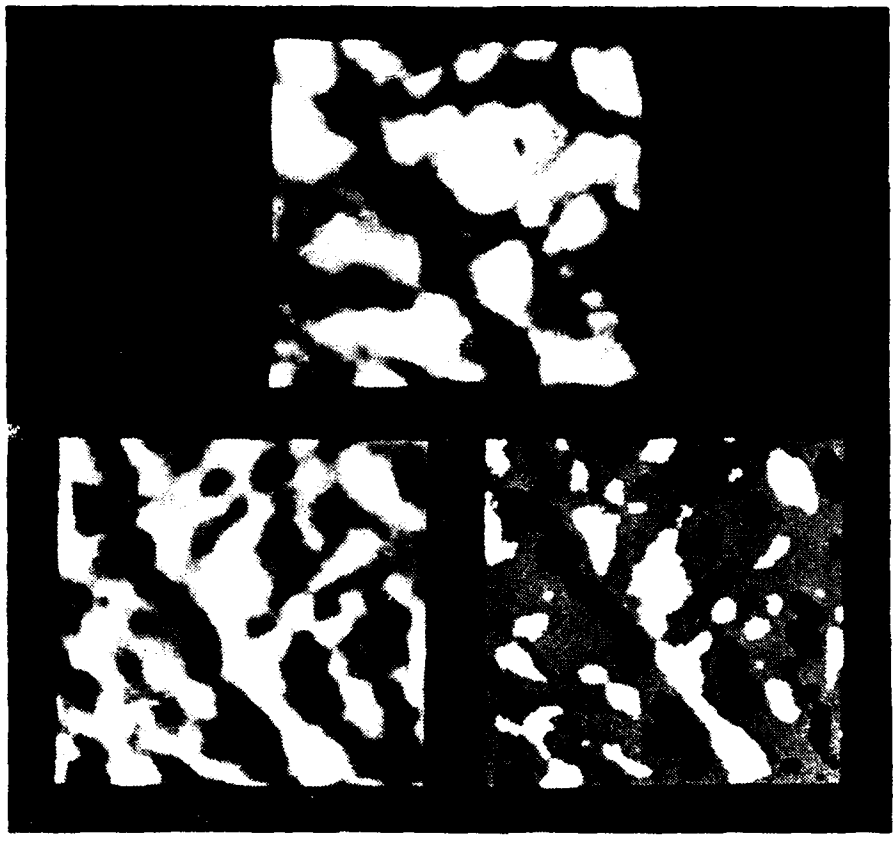

Fig. 2

A 10x10 arc second section of the solar surface (top). A difference mask generated by shifting the picture 0.7 arc seconds to the left and right and subtracting (lower left). Same as before, but with only three transmittance levels 0, 0.5 and 1 (lower right).

wavefront gradient can be measured by using a detector array in P', and, if the gradient in the orthogonal direction is also known, the wavefront can be reconstructed by using standard integration algorithms.

It is shown in von der Lühe (1987) that the intensity distribution $P(\mathbf{z})$ in the pupil image P' is approximately given with:

$$P(\mathbf{z}) \approx B^2 F(0) + 4BC \overline{|F(\sigma/2)|^2} \sin(\phi(\mathbf{z}) - \phi(\mathbf{z} - \sigma/2)) \qquad (2)$$

$\mathbf{z}$ is a two-dimensional pupil plane coordinate. $F(\mathbf{z})$ is the Fourier transform of $I(\mathbf{x})$. $\phi(\mathbf{z})$ denotes the wavefront deformation at pupil coordinate $\mathbf{z}$. The term $\overline{|F(\sigma/2)|^2}$ represents an integral:

$$\overline{|F(\sigma/2)|^2} = \int\int_{HP} |F(\mathbf{z})|^2 \sin\pi\Delta\mathbf{z} \, d\mathbf{z} \qquad (3)$$

HP is the half plane in Fourier space limited by a straight line perpendicular to the Δ-direction and through the frequency origin. The "effective shear" σ results from the product of the power spectrum and the sine term in eqn. (3). Fig. 3 represents the power

spectrum, the sine term and the product.

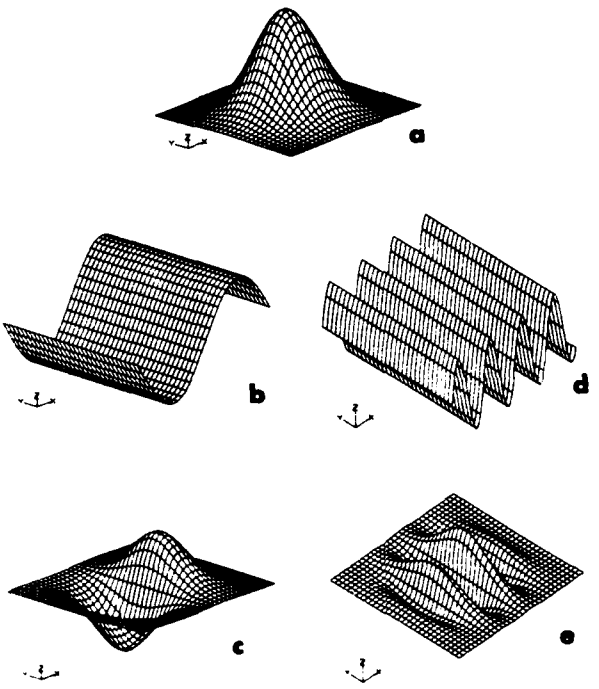

Fig. 3

The integrand of eqn. (3). (a) represents the power spectrum of a bandlimited target structure. (b) shows the sine term when Δ is the correlation length, (d) if Δ is appreciably larger. (c) and (e) show the corresponding products. (c) is the effective operator used to generate wavefront differences. With (d), no local wavefront gradients can be obtained.

The shear σ is given by the separation of the two extrema in the product shown in fig. 3c. Hence, σ is determined by both the equivalent width of the power spectrum which, in turn, is related to the correlation scale of the target structure, and the mask shift Δ. As a rule of thumb, Δ should match the correlation scale of the target structure in order to make the device most efficient.

If wavefront errors are small compared to $\pi/2$, eqn. (2) can be linearized:

$$P(\mathbf{s}) \approx B^2 F(0) + 4BC \overline{|F(\sigma/2)|^2} (\phi(\mathbf{s}) - \phi(\mathbf{s} - \sigma/2)) \qquad (4)$$

This equation holds when an adaptive system operates close to zero wavefront error.

In the real world, one will have to take precautions against intensity fluctuatuins caused by, e. g., scintillation. Those would be interpreted as global or local wavefront tilts, produce wavefront fitting errors and may drive a corrective system out of its range. One possibility to eliminate intensity fluctuations is to make two measurements of the pupil intensity with two masks that have opposite contrast. The transmitance m' of the

inverted contrast mask is given with:

$$m'(\mathbf{x}) = B + C \left(I(\mathbf{x} + \Delta) - I(\mathbf{x} - \Delta) \right) , \tag{5}$$

and the pupil intensity distribution caused by m' is for small wavefront errors:

$$P'(\mathbf{z}) \approx B^2 F(0) - 4BC \overline{|F(\sigma/2)|^2} \left(\phi(\mathbf{z}) - \phi(\mathbf{z} - \sigma/2) \right) \tag{6}$$

The difference $P - P'$ is independent of overall fluctuations in intensity:

$$P(\mathbf{z}) - P'(\mathbf{z}) \approx 8BC \overline{|F(\sigma/2)|^2} \left(\phi(\mathbf{z}) - \phi(\mathbf{z} - \sigma/2) \right) \tag{7}$$

3. Numerical simulations

The performance of the method is demonstrated in one-dimansional simulation calculations. Fig. 4a presents a one-dimensional object distribution, the pattern was chosen to model solar granulation with 8% contrast.

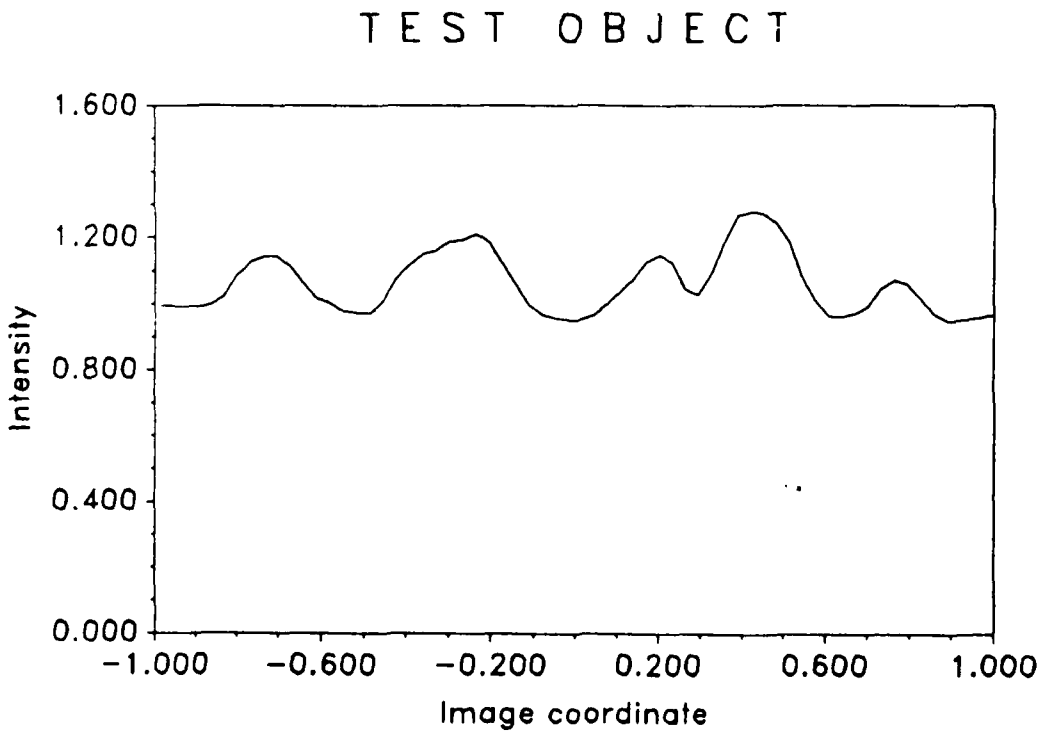

Fig. 4a

The sampling matches the resolution of a 70cm telescope at a light wavelength of 500nm, the field corresponds to 9.6 seconds of arc. Fig. 4b shows three sample waveforms used to aberrate the focal plane image. The dashed line represents a quadratic wavefront error term (defocus), the dot-dashed line a third-order coma term and the solid line a random

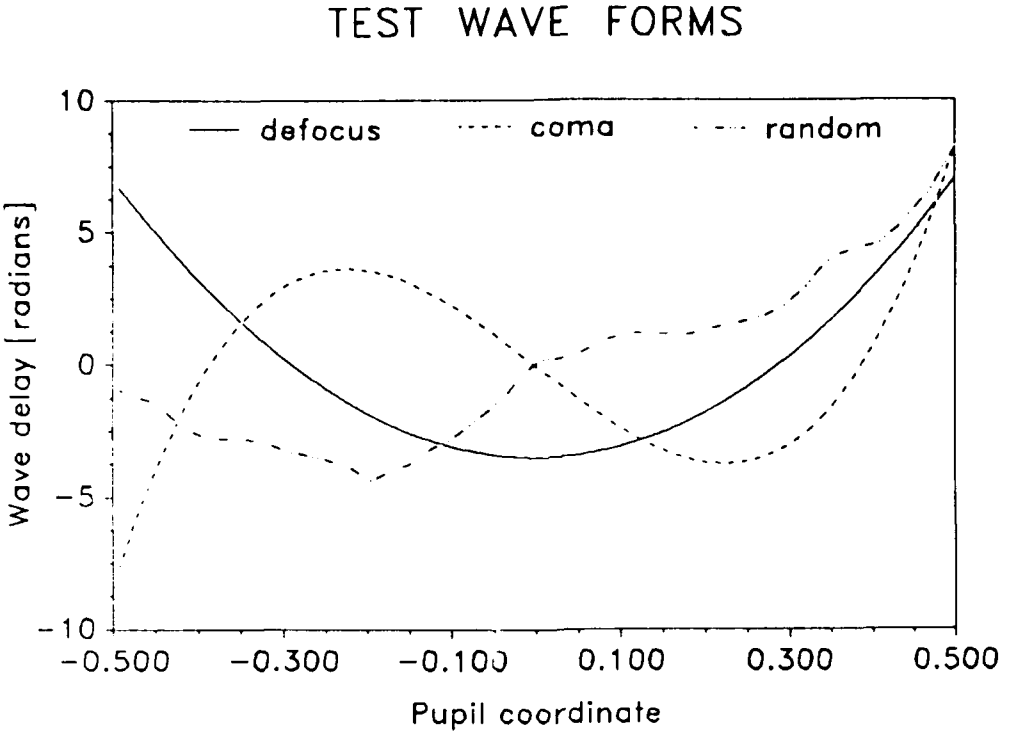

Fig. 4b

wavefront aberration with second-order statistics corresponding to those caused by atmospheric turbulence. Fig. 5 shows point spread functions for all three wave forms and for values of rms wavefront error ranging from minus to plus two waves. Fig. 6 presents the results. The first column of surface plots represents the one-dimensional pupil plane intensity as a function of rms wavefront error, for all three waveforms. The second column presents the intensity difference (eqn. (7)) for mask measurements with inverted contrast. The third column presents the "reconstructed" waveform, calculated by integrating the differences from the second column.

It is apparent that the signal in the pupil image is relatively low, it is of the order of the contrast of the target structure (first column). The pupil intensity difference (second column) reveals the non-linearity of the response, as expressed in eqns. (2) and (6). The reconstructed waveforms, however, still have much resemblance with the input waveforms, even for large rms wavefront errors, except for sections where the wavefront gradient is very large. One should keep in mind, however, that the "reconstructed" wavefront would be the initial response of an adaptive system to a measured error and in all cases, the errors will be substantially reduced so the system would quickly acquire a zero wavefront error state during further iterations. It is important that the system reliably detects the null state of the wavefront error and otherwise maintains its proper sign;

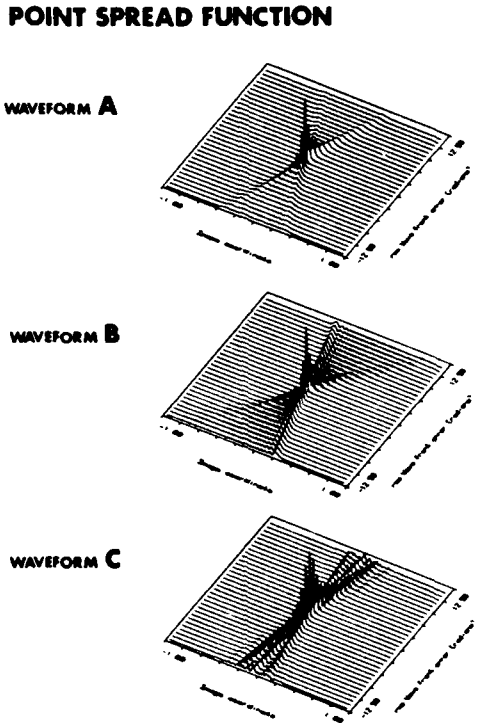

Fig. 5

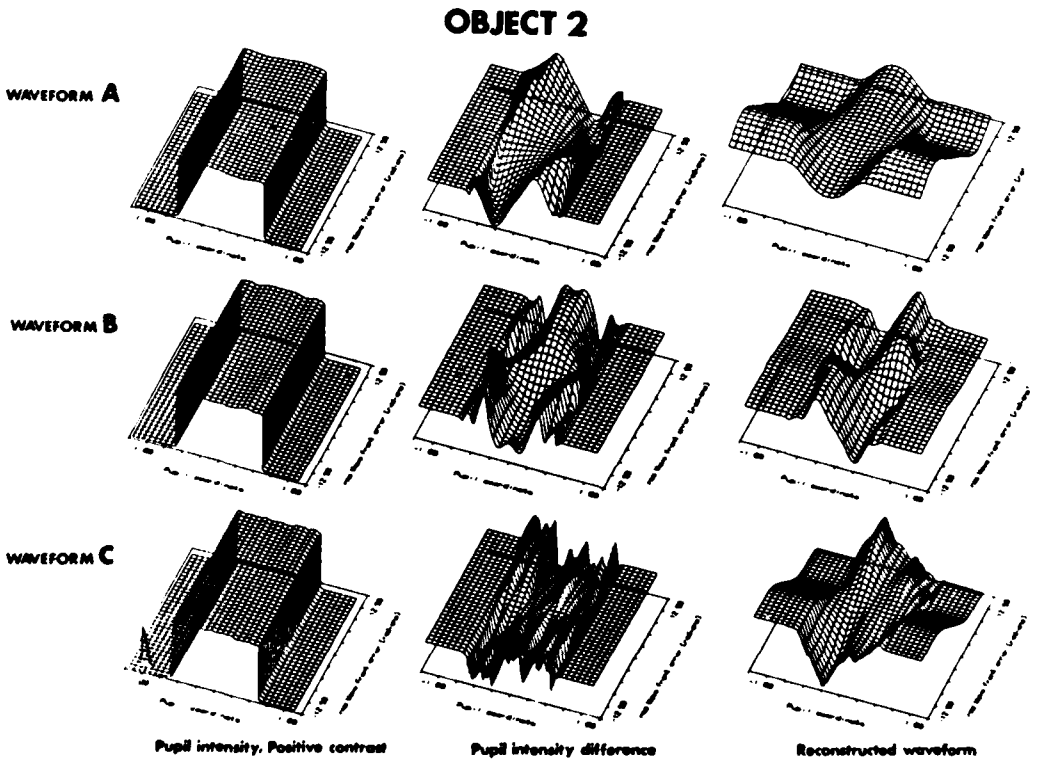

Fig. 6

nonlinearities of the response are only of minor concern.

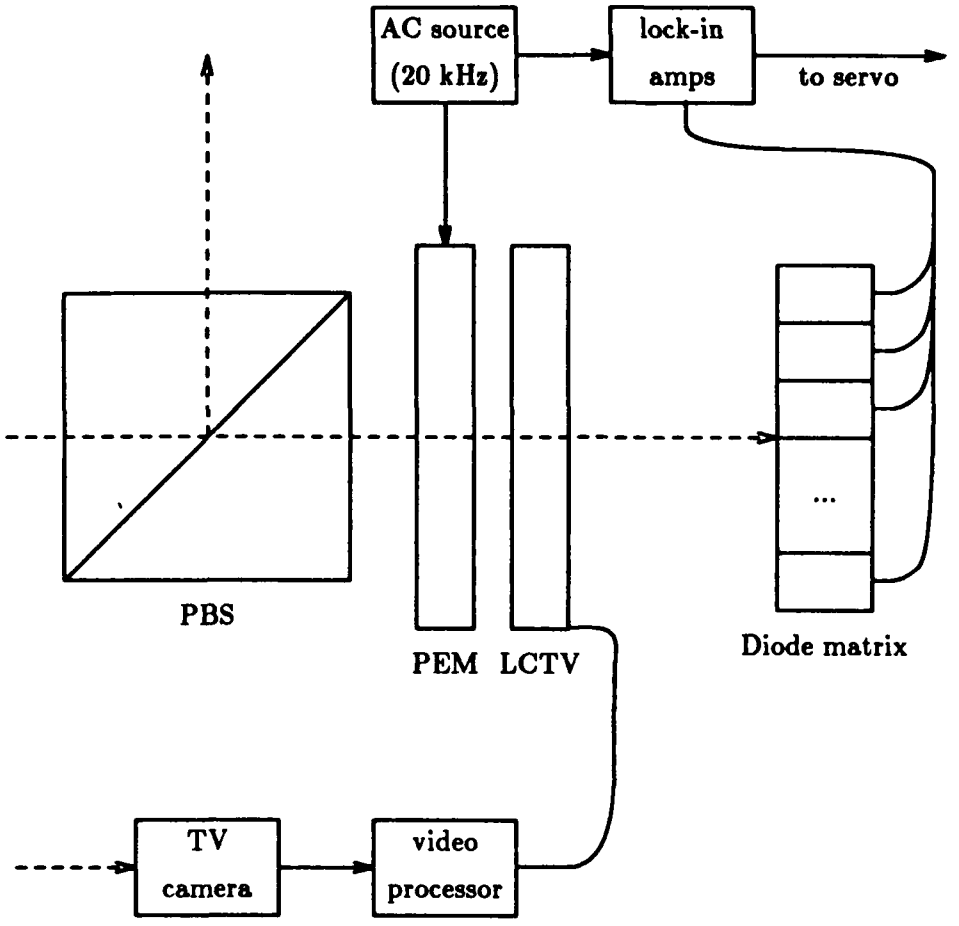

Fig. 7

4. Implementation of the method into a solar wavefront sensor

A wavefront sensor will consist of two masks which have linear independent, preferrably orthogonal, shifts Δ and Δ'. A possibility to generate transparent masks is given by optical modulators commonly used in photonics research. A particularly inexpensive approach might be the implementation of liquid-crystal pocket TV's (LCTV's). They make good optical modulators, with 20:1 contrast in white light, but their pixel size might be somewhat large (0.1mm) which results in a bulky optical setup.

One way to construct a LCTV-based wavefront sensor is shown in fig. 7. A polarizing beam splitter is used to generate two focal planes in linear polarized light for the two masks; only one is shown in the figure. A modified LCTV, where the polaroids have been stripped from both sides, is placed in the focus. A piezo-elastic modulator (PEM) is placed before the LCTV; the modulator serves to rotate the plane of polarization by 90 degrees back and forth at a high rate, say, 20 KHz. The liquid crystal rotates the plane of

polarization further, depending on the video signal at the pixels. An analyzer is placed following the LCTV which converts the polarization modulation into modulation of intensity. The modulator acts as a contrast inverter in conjunction with the analyzer, the video picture on the LCTV is constantly contrast inverted at the modulation frequency.

Additional optics that are not shown reimage the telescope's entrance pupil onto a diode matrix. Each diode samples an area of the size of the desired subaperture, there are as many discrete diodes as there are subapertures in the pupil. Intensity fluctuations are measured here; because of the modulation the intensity fluctuations are offset at the modulation frequency. This facilitates their detection because DC offsets in the diode preamps are thrown out. Lock-in amplifiers serve to demodulate the signals; they now represent local wavefront tilts and they are sent to the servo system which controls the active device.

The LCTV is driven by a video camera located at a third focal plane and followed by a video processor which generates the necessary difference pictures. The difference pictures are generated from long exposure averages which are updated every 30 $\cdots$ 60 s.

Alternatively, the analyzer behind the LCTV can be replaced by another polarizing beam splitter followed by a second diode matrix in the pupil image in order to save light. This approach would make the setup somewhat more complex.

5. Signal magnitude and noise considerations

We shall discuss photon noise in this section only. The required signal magnitude can be estimated by asking how many photons are necessary to detect and maintain the zero wavefront error state to a given precision. The signal for wavefront errors close to zero is given by eqn. (7), if difference measurements are made. We shall now make estimates for the various factors that enter this equation and compare the signal with the bias term in order to obtain the relative intensity variation.

B: average mask amplitude transmittance = 0.5.

C: mask contrast; depends on the typical rms contrast C_{rms} of a long exposure granulation picture. Under average seeing conditions, we will have $C_{rms} = 0.03$. If Δ is half the correlation scale (0.7 arc sec), then the difference image will also have about 3% rms contrast, or 10% peak-to-peak. Thus, C = 10 if the full range of the mask is used.

$\overline{|F(\sigma/2)|^2}$: power integral in eqn. (3). The integral of the entire power spectrum $|F(\mathbf{x})|^2$ is $(0.03)^2 \approx 10^{-3}$; a factor 1/2 applies because the integration is carried out over half the Fourier plane only. The sine factor in eqn. (3) can be accounted for by another factor 1/2 $\rightarrow$ $\overline{|F(\sigma/2)|^2} = \frac{1}{4} C_{rms}^2 \approx 2.5 \times 10^{-4}$.

We have to compare the result $\tilde{P}(\mathbf{x}) = P(\mathbf{x}) - P'(\mathbf{x})$ with the average pupil intensity sum $\Sigma = 2B^2\overline{I}$. Hence, an estimate of the intensity difference is given with:

$$\frac{\tilde{P}(\mathbf{x})}{\Sigma} = 2 \times 10^{-2} \left(\phi(\mathbf{x}) - \phi(\mathbf{x} - \sigma/2)\right) = 2 \times 10^{-2} \Delta\phi(\mathbf{x}) \qquad (8)$$

If we require that the signal is photon noise limited, we obtain a minimum number of detected photons for various rms wavefront errors, as shown in table I.

We now make an estimate of the number of available photons. The area of a subaperture, i. e., the area subtended by a single detector in the pupil (cf. fig. 7) has to be at least so large that the target structure (granulation) can be resolved. Let us assume a resolution of 1.5 seconds of arc, which corresponds to a subaperture of 7cm in diameter. There are 1.7×10^9 photons $\text{Å}^{-1}\ \text{s}^{-1}$ per resolution element in the visible at about 500nm, this number increases with the size of the sensor field of view. If we allow for a wavelength range of 200 Å, sample with a 2KHz rate and account for light losses in the wave front sensor (2 polarizers, various surfaces, detector quantum efficiency etc.) with a factor 1/10, we arrive at total photon numbers that are shown in table II. The fraction of light needed from the main optical beam for the wavefront sensor working photon noise limited is shown in table III.

Table I

rms WFE	$\Delta\phi$ [rad]	$\tilde{P}/\Sigma$	minimum # photons $(\Sigma/\tilde{P})^2$
$\lambda/10$	0.628	1.3×10^{-2}	5.9×10^3
$\lambda/20$	0.314	6.3×10^{-3}	2.5×10^4
$\lambda/50$	0.126	2.5×10^{-3}	1.6×10^5

Table II

sensor field size [arc sec]	# photons in field [*angstrom*$^{-1}$ *s*$^{-1}$]	# photons per measurement 200 Å, 5×10^{-4} *s*
2 x 2	3.0×10^{9}	3.0×10^{7}
5 x 5	1.9×10^{10}	1.9×10^{8}
10 x 10	7.6×10^{10}	7.6×10^{8}

Table III

sensor field size	Fraction of light used for WFS, at rms WFE		
[arc sec]	$\lambda/10$	$\lambda/20$	$\lambda/50$
2 x 2	2×10^{-3}	8×10^{-3}	5×10^{-2}
5 x 5	3×10^{-4}	1×10^{-3}	8×10^{-3}
10 x 10	7×10^{-5}	3×10^{-4}	2×10^{-3}

6. Conclusions

The discussion in the previous section shows that the proposed wavefront sensor is very efficient. Between 0.1% and 5% of the light is needed for the sensor to operate photon-noise limited under all conceivable situations. Even if we account for additional, instrumental noise the amount of light needed still might be about as low as 10%.

Some comments are now in order to prevent undue criticism. First, effects of anisoplanatism are not considered here. It is understood that anisoplanicity poses a severe problem, and it is not guaranteed that the proposed method will work satisfactorily if the field is cut down to approximately the correlation scale of the target structure. Much more detailed study is necessary to understand all the effects that might arise from such a situation; the previous, crude analysis is certainly insufficient. But the technique should work with fields as small as 5 arcsec, which matches the typical size of an isoplanatic patch. Similar problems will arise with any kind of wavefront detection using solar granulation as target structure.

Second, one might argue that a subaperture size of 7cm is too large for average seeing conditions, so the sensor will sucessfully operate under good seeing conditions only. One has to keep in mind, however, that wavefront slope measurement are made and pure wavefront tilt is a good wavefront error approximation to a 7cm region if r_o is as small as

4cm! (This is, by the way, true for any kind of slope measurement). In fact, the proposed technique will operate over a large range of seeing conditions, with only the worst cases excluded.

Acknowledgements: It is a pleasure to thank Richard B. Dunn for discussions that stimulated the idea, for his continuous input and his great interest in this work. This work was done while the author held a National Research Council / Air Force Geophysics Laboratory Resident Research Associateship.

Literature

von der Lühe, O. (1986), "A Wavefront Error Measurement Technique using Extended, Incoherent Light Sources," subm. to *Optical Engineering*